Semiconductor Halogenation in Molecular Highly-Oriented Layered p–n (n–p) Junctions

Iulia Cojocariu,* Matteo Jugovac, Sidra Sarwar, Jeff Rawson, Sergio Sanz, Paul Kögerler, Vitaliy Feyer,* and Claus Michael Schneider

Organic p–n junctions attract widespread interest in the field of molecular electronics because of their unique optoelectronic singularities. Importantly, the molecular donor/acceptor character is strongly correlated to the degree of substitution, e.g., the introduction of electron-withdrawing groups. Herein, by gradually increasing the degree of peripheral fluorination on planar, D_{4h}–symmetric iron(II) phthalocyanato (FePc) complexes, the energy level alignment and molecular order is defined in a metal-supported bilayered Pc-based junction using photoemission orbital tomography. This non-destructive method selectively allows identifying molecular levels of the hetero-architectures. It demonstrates that, while the symmetric fluorination of FePc does not disrupt the long-range order and degree of metal-to-molecule charge transfer in the first molecular layer, it strongly impacts the energy alignment in both the interface and topmost layer in the bilayered structures. The p–n junction formed in the bilayer of perhydrogenated FePc and perfluorinated $FeF_{16}Pc$ may serve as an ideal model for understanding the basic charge-transport phenomena at the metal-supported organic–organic interfaces, with possible application in photovoltaic devices.

I. Cojocariu, M. Jugovac, S. Sarwar, J. Rawson, S. Sanz, P. Kögerler,
V. Feyer, C. M. Schneider
Peter Grünberg Institute (PGI-6)
Forschungszentrum Jülich GmbH
52428 Jülich, Germany
E-mail: i.cojocariu@fz-juelich.de; v.feyer@fz-juelich.de
I. Cojocariu, M. Jugovac
Elettra-Sincrotrone
S.C.p.A, S.S 14 – km 163.5, 34149 Trieste, Italy
S. Sarwar, J. Rawson, P. Kögerler
Institute of Inorganic Chemistry
RWTH Aachen University
52056 Aachen, Germany
V. Feyer, C. M. Schneider
Fakultät f. Physik and Center for Nanointegration Duisburg-Essen
(CENIDE)
Universität Duisburg-Essen
47048 Duisburg, Germany
C. M. Schneider
Dept. of Physics and Astronomy
UC Davis
Davis, CA 95616, USA

1. Introduction

Metallic contacts in organic optoelectronic devices determine their ultimate performance.[1] Therefore, to define the properties of devices with organic components, like light-emitting diodes (LEDs), photovoltaic (PV) cells, and ambipolar field-effect transistors (FETs), one has to consider the intrinsic properties of the metal substrate, like transparency, reactivity, and work function. As demonstrated by several groups, the work function of the metal can be tuned by depositing molecules that form a highly ordered, thin, 2D layer that has a dipole in the desired direction.[2–4] As an example, alkanethiols and perfluorinated alkanethiols are known to form such self-assembled monolayers (SAMs)[2,5–7] on metals, and since they have opposite dipoles, they can be used to, respectively, decrease and increase[2] the work functions of metals (i.e., shift the vacuum energy levels).[8] Besides using the dipoles of SAMs to tune metal work functions, the interface dipole formed by SAMs can control the charge-carrier density in organic FETs.[3,9] We note that the formation of a second layer in thiol-based hetero p–n junctions is not trivial due to their autophobic behavior.

Metal phthalocyanine (MPc) compounds are often used to frame SAMs because of their structural stability and commercial availability. The controlled modification of peripheral substituents, e.g., the halogenation of Pc, in particular fluorination, is a well-established method to tune electron transport. It is known that, in order for an organic material to transport electrons with large charge-carrier mobility (n–type), it needs to have an accessible low-energy unoccupied molecular orbital (LUMO) for electron injection and sufficient π–overlap between molecules.[10] Therefore, molecules with strong electron-withdrawing groups and extended π–systems are good candidates as n-channel semiconductors.[11] A rectifying junction could then be formed with p–type unsubstituted MPc molecules.[12–14]

It often remains challenging to form molecular heterostacks where n- and p-type layers alternate in a well-defined manner. Indeed, on weakly interacting substrates, where the molecules are only physisorbed, intermixed phases are usually formed upon deposition of the second layer.[15] To avoid such an effect, one solution might be to enter the regime of chemisorption, where the strong interaction at the molecular-substrate interface can be effectively used to suppress the

**ADVANCED
SCIENCE NEWS**

www.advancedsciencenews.com

**ADVANCED
FUNCTIONAL
MATERIALS**

www.afm-journal.de

molecular rearrangement and avoid possible interlayer mixing effects, thus allowing well-defined heterostacks to form. We show hereafter, how the strong interaction between the silver supporting electrode and the first layer of iron phthalocyanines, independently of the degree of fluorination, enables the formation of a robust template for building up well-defined organic hetero-architectures.

In the past, FePc molecules and their derivatives, self-assembled in sub-monolayer and monolayer (ML) coverages on metal and oxide surfaces, have been already intensively studied by a variety of surface-sensitive techniques, among them scanning tunneling microscopy (STM),[16] photoelectron spectroscopy (PES),[17] and near-edge X-ray absorption fine structure (NEXAFS).[18] Although these integrated surface analysis methods are sensitive, they cannot be readily applied to study the multilayer systems and organic–organic interfaces because they do not selectively probe each molecular layer individually. Therefore, a non-destructive technique that investigates each layer individually is desirable for heterolayered organic systems, especially considering the potential of phthalocyanine-based organic heterostructures in organic device applications.[19] In the present work, we prove photoemission tomography (PT) as a method that very well matches these requirements and presents itself as a perfect non-destructive tool to study the impact of fluorination on the electronic and structural properties of different FeF_xPc molecules in both monolayer and bilayer regimes. Thanks to the well-distinguishable highest occupied molecular orbital (HOMO) features associated with the interface and the topmost layer, we use PT to study the electronic level alignment, azimuthal orientation as well as the contact angle in the molecular bilayer systems, disentangling the contribution of each layer in the stacked molecular (p–n) heterojunctions with no erosion or other processes required unlike in the case of STM measurements.[20]

In particular, we observe that in the case of homobilayered stacks of FePc, the LUMO level in the first layer is fully filled by the charge transfer from the metal substrate, while the FePc in the second layer is fully decoupled from the substrate and no charge transfer is manifested. Interestingly, fluorination does not influence the charge transfer at the interface. However, in homobilayered structures of fluorinated FeF_xPc molecules, those in the second layer are oriented differently compared to the first one. Moreover, depending on the order of deposition of perhydrogenated FePc and perfluorinated $FeF_{16}Pc$, well-defined n–p and p–n junctions have been successfully designed and their intrinsic electronic properties at molecular level have been characterized by photoemission spectroscopy. These uniform bilayer stacked structures with well distinct n/p type organic semiconductor layers can be used in future molecular-based PV devices.

2. Results and Discussion

2.1. Energy Level Alignment and Molecular Arrangement in FeF_xPc Monolayers

The first step toward the fabrication of bilayer structures is to obtain an ordered first layer characterized by sufficient interaction with the surface for interlayer mixing to be avoided. We

thereby study in the present section the molecular order and energy alignment of the phthalocyanine monolayer on Ag(110). Having in mind that atom substitution, such as fluorination, can tune the interactions in the assembled molecular layer, three different molecules, with a increasing degree of peripheral fluorination, FePc, FeF_8Pc, and $FeF_{16}Pc$, all of which are charge–neutral, have been assembled on the metal electrode.

XPS is employed here to demonstrate that the stoichiometry of each compound is preserved after deposition upon the surface. **Figure 1**a shows the C 1s core-level spectra of the FeF_xPc monolayers on Ag(110). Three main components are used to deconvolute the spectra, which correspond to carbon atoms bonded to other carbon atoms (C−C), carbon atoms bonded to nitrogen atoms (C−N), and carbon atoms bonded to fluorine atoms (C−F). For each component, a shake-up satellite peak was added at 1.2 ± 0.1 eV from the main component. The relative peak areas, labeled as I_{CC}, I_{CN}, and I_{CF} for the above-mentioned components, are in good agreement with the stoichiometry of the considered molecules. $I_{CF}:I_{CN}:I_{CC}$ ratio is 0:1:3, 1:1:2 and 2:1:1 for FePc, FeF_8Pc, and $FeF_{16}Pc$, respectively.

The identity of the adsorbate and ordering at the interface influence the vacuum level alignment. These changes can be appreciated by measuring the difference between the metal work function ($\Delta\Phi_{Ag}$) before and after deposition of a saturated monolayer, determined by measuring the secondary electron cutoff of the bare metal and the monolayers (see Figure 1b). While a monolayer of FePc decreases the WF ($\Delta\Phi_{Ag} = -0.2$ eV), increasing the electron affinity, $FeF_{16}Pc$ monolayer increases it ($\Delta\Phi_{Ag} = +0.35$ eV), leading to the lowering of the hole-injection barrier. Deposition of FeF_8Pc does not significantly perturb the metal WF. All the variations in the work function, $\Delta\Phi_{Ag}$, can be linked to surface dipole variations induced by molecular adsorption, which depending on the molecular dipole at the surface created at the organic/metal interface, may have positive or negative signs.[21–23] The molecular dipole at the organic/metal interface is localized foremost at the first molecular layer, and the sign of the dipole moment of the fluorinated molecule is opposite to that of the non-fluorinated one.[23] This often causes the energy shift of former LUMOs below the Fermi level.[24]

We measured the UV photoelectron spectra (UPS) of FePc/Ag(110), FeF_8Pc/Ag(110), and $F_{16}FePc$/Ag(110) interfaces as well as the bare Ag(110). While the valence band spectrum of the bare Ag(110) substrate shows a rather featureless plateau associated with the silver sp-bands, prominent molecular features appear in the three molecular/metal interfaces (see Figure 1b). Interestingly, the spectra of the molecular films show two prominent features at 0.48 and 1.30 eV binding energy (BE). To identify the origin of the features observed in the spectra, we have measured 2D momentum maps at corresponding BE values for the three interfaces reported in Figure 1c. Next, the experimental data have been compared to the square modulus of the Fourier transform (FT) of the real space molecular orbitals calculated for the gas-phase FePc, FeF_8Pc, and $F_{16}FePc$ molecules within the PT approach.

Within the PT approach, photoelectrons emitted from an orbital in the full half-space above the sample are collected and recorded according to their momentum distribution. This leads to so-called momentum maps, which are tomograms of the momentum distribution of the molecular orbitals.[25,26] The direct comparison of the momentum maps with the square
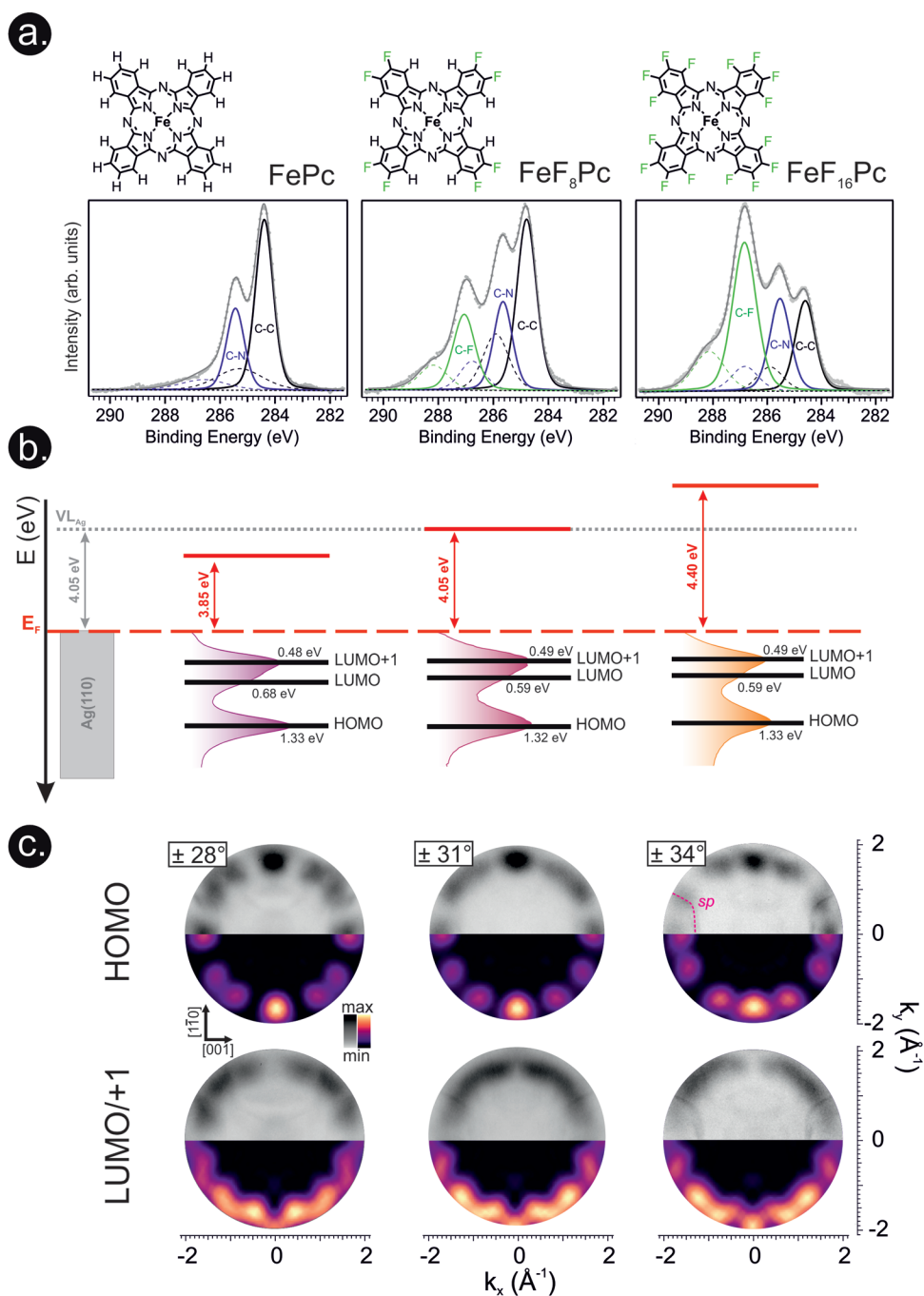
2208507 (2 of 8)

Figure 1. XPS C 1s core level spectra, along with the deconvoluted components (a), energy level diagram referred to the clean Ag(110) substrate (b) and comparison between experimental (top half) and simulated momentum maps (bottom half) on the HOMO and LUMO/LUMO+1 levels (c) for FePc, FeF$_8$Pc, and FeF$_{16}$Pc monolayers deposited on Ag(110). Ag sp-band position marked by dashed line.

modulus of the FT allows to unambiguously assign the photoemission features to molecular orbitals and to accurately determine the azimuthal orientation and the tilt angle of the molecule. In the past, the PT approach has been already successfully employed to study the geometry and electronic structure of molecular semiconductors, such as metal porphyrins and phthalocyanines, in self-assembled single-layered arrays on metal substrates.[27–29] From Figure 1c, we note that the resemblance of simulated and measured HOMO state of a$_{1u}$ symmetry (BE = 1.30 eV) and two degenerate LUMO/LUMO+1 states of e$_g$ symmetry (BE = 0.48 eV) is clear; thus, the emission peaks can be assigned to the two molecular states of MPcs. The adsorption onto the silver substrate lowers the HOMO-LUMO energy gap to 0.82 eV, substantially reduced compared to the isolated molecule, where theoretically, a value of 1.58 eV has been reported.[30]

**ADVANCED
SCIENCE NEWS**

www.advancedsciencenews.com

**ADVANCED
FUNCTIONAL
MATERIALS**

www.afm-journal.de

Moreover, the detection of the LUMO confirms that electron donation from the metal to the LUMOs of FePc and $FeF_{16}Pc$ is similar independently of the molecular fluorination, while the WF manifests a difference of ≈0.45 eV between these two systems, rising from the different molecular polarity.

The experimental patterns are shown in the top half panels of Figure 1c. In addition to the features originating from the molecular states, it also contains sharp *sp*-band contributions from the Ag(110) surface (visible at $|k_x| \approx 1.2$ Å^{-1}). Exploiting these features of the Ag substrate as a gauge in the momentum maps and comparing the calculated and measured momentum maps, the azimuthal orientation of the molecule with respect to the substrate's high symmetry directions can be determined, allowing us to probe the effect of H···H and F···F steric repulsions at the monolayer/substrate interface. Moreover, the symmetry of the Ag(110) substrate leads to two mirror domains with oppositely tilted azimuthal angles of the molecules, and as a consequence, both of them must be taken into account for the simulated patterns. The best agreement between all experimental and corresponding simulated momentum maps is found for an azimuthal orientation of FePc, FeF_8PC, and $F_{16}FePc$ of ±28°, ±31°, and ±34° relative to the [1$\bar{1}$0] direction of the substrate, respectively, with the molecules lying parallel to the surface (tilt angle 0 ±5°, see Figure S1, Supporting Information). The result depicted from molecular maps for FePc/Ag(110) interface agrees well with the previously published STM data.[20] Notably, the gradual increase of the degree of fluorination induces a continuous increment of the azimuthal angle (+3°) in an effort to minimize the intermolecular repulsions.

Structural ordering at the saturated monolayer regime has been evaluated by means of low energy electron diffraction (LEED) patterns acquired at a fixed incidence electron energy of 14 eV for the three systems under investigation. In all molecular systems, the superstructure is commensurate and the relative matrices are reported in **Figure 2**. The increased degree of fluorination leads to the increase of the azimuthal angle and area of the unit cells in order to minimize intermolecular steric repulsions.

The expansion of the unit cell area with respect to the FePc (188.82 Å^2) is 12.5% (212.39 Å^2) and 25% (236.03 Å^2) for FeF_8Pc and $FeF_{16}Pc$, respectively. The area increment between the perhydrogenated system and the perfluorinated one is comparable to the increase in the van der Waals radius (1.20 Å for H and 1.47 Å for F).[31]

2.2. Layered Homojunctions

By depositing a second layer of compound atop the first well-defined homojunctions may be fabricated. The energy level realignment in the homojunction and the molecular ordering on the topmost layer are discussed in the following. To address these points, we performed valence band measurements, in particular PT mapping and WF determination, for FePc, FeF_8Pc, and $FeF_{16}Pc$ molecules in the homobilayer films supported by the Ag(110) surface (see **Figure 3**). As mentioned above, the PT approach is one of the best-suited methods for determining the azimuthal angle and energy level alignment of molecules in the topmost as well as in the interfacial layer in the bilayer
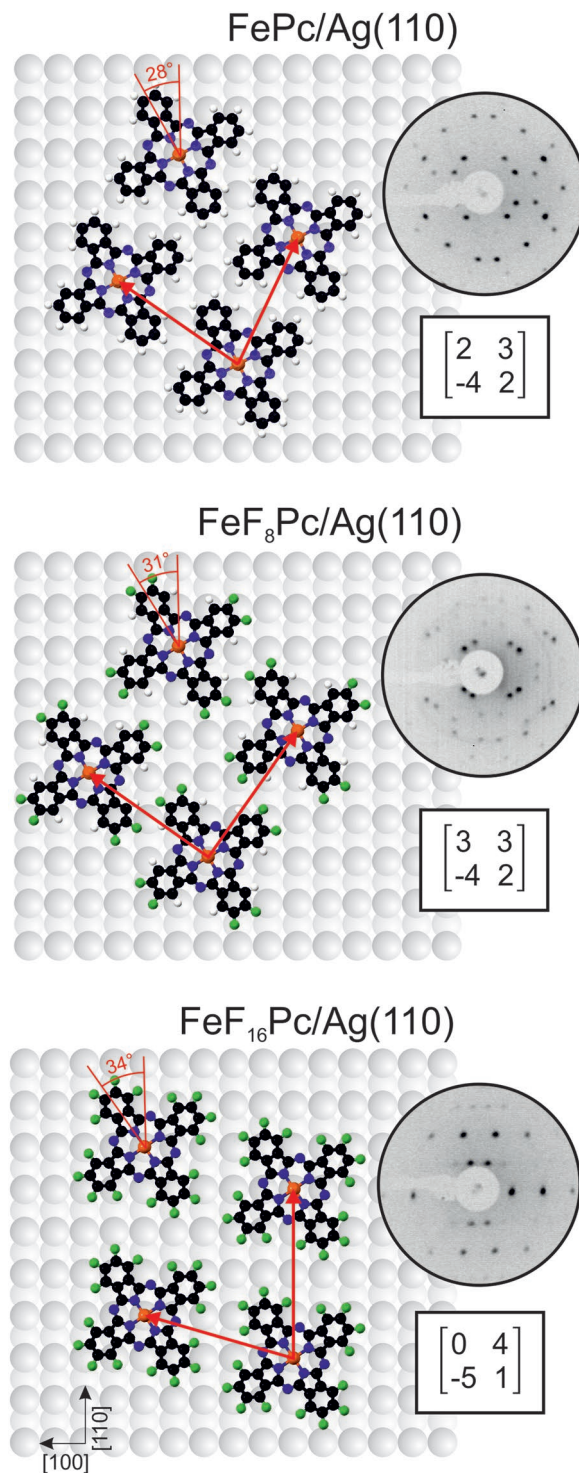

Figure 2. Sketch of the superstructure ordering, relative LEED pattern acquired at 14 eV and derived superstructure matrix for the self-assembled monolayers of FePc, FeF_8FePC, and $FeF_{16}Pc$ on Ag(110).

systems,[32] with no erosion or other processes required unlike in the case of STM measurements.[20] Indeed, the features associated with the HOMOs of the first (HOMO) and second layer (HOMO$_{bil}$) are well separated in energy (see Figure 3).
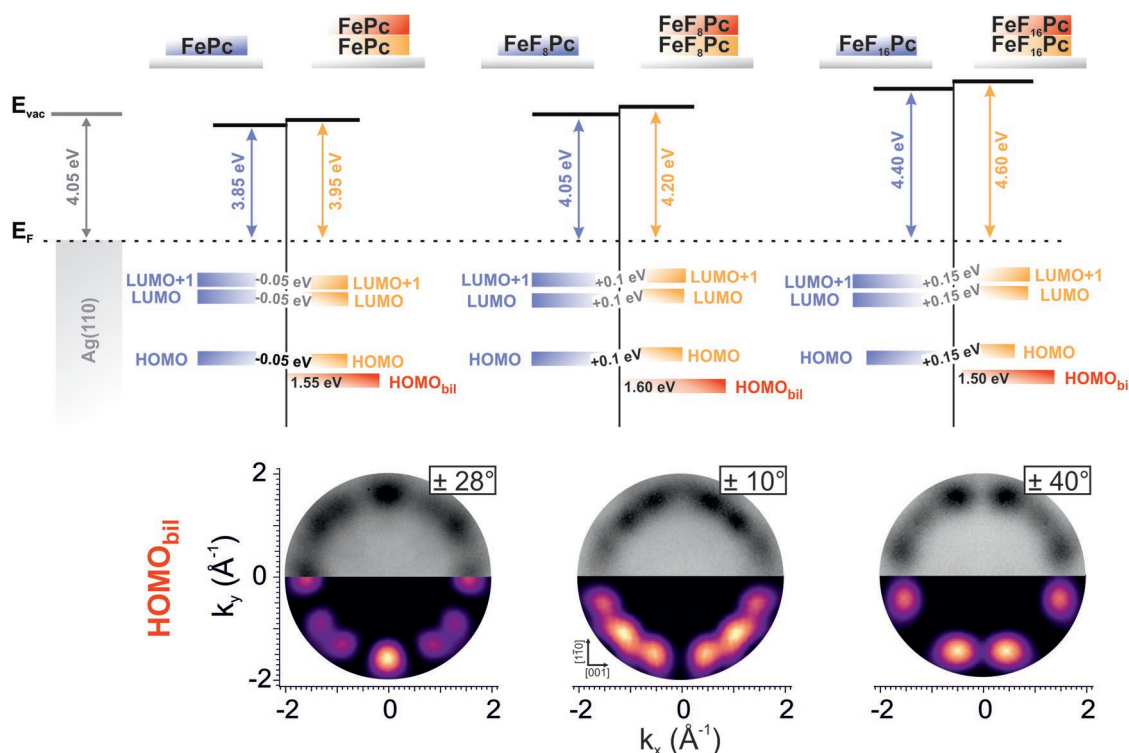
Figure 3. Energy level diagram referred to the clean Ag(110) substrate (top) and comparison between experimental and simulated momentum maps on the $HOMO_{bil}$ level (bottom) for FePc, FeF_8Pc, and $FeF_{16}Pc$ homobilayers deposited on Ag(110).

The formation of the bilayered homojunction induces a vacuum level realignment, evidenced by the changes in the work function value, which incrementally increases with the degree of halogenation; variations from 100 to 200 meV are observed on the FePc and the $FeF_{16}Pc$ bilayers, respectively. The presence of the second layer also induces energy shifts on molecular levels of the first layer, despite its strong coupling to the silver electrode. In the absence of fluorination, the bottom FePc layer exhibits a downshift in energy by 50 meV in the presence of the second layer. On the other hand, a second layer of FeF_8Pc shifts the levels of the underlying layer by 100 meV, and for $FeF_{16}Pc$ the upshift is by 150 meV.

At the same time, the first layer in direct contact with the metal electrode acts as a decoupling layer for the topmost layer, effectively screening it from the substrate. No occupation of the LUMO is observed on the second layer, and only the feature labeled as $HOMO_{bil}$ rises in the spectra as a consequence of the additional deposition. Moreover, the absence of the LUMO peak for the second layer clearly indicates that the HOMO-LUMO gap for both FePc and $FeF_{16}Pc$ systems in the topmost layer is larger than the underlying layer directly contacted with metal substrate.

To determine the stacking geometry of the FeF_xPc bilayer systems, we have measured molecular maps of $HOMO_{bil}$ of the molecules in the topmost layer and determined the azimuthal angle in order to compare them with the ones obtained previously for the monolayer system (see Figure 3).

Substantial differences in the molecular arrangement are observed in the second layer. The azimuthal angles change drastically in the case of the fluorinated FeF_8Pc and $FeF_{16}Pc$

second layer, while the FePc second layer preserves the order register of the first underlying layer, in agreement with STM measurements on the FePc bilayer.[20] The azimuthal angle of ±10° observed for the bilayered FeF_8Pc, where the periphery is occupied by both hydrogen and fluorine, suggests that the second layer absorbs in such a way as to avoid any proximity between groups of the same nature, with the fluorine atoms sitting on top of the hydrogen present on the first layer and vice versa.

2.3. Layered Heterojunctions

By depositing a layer of perhydrogenated FePc atop perfluorinated $FeF_{16}Pc$ (n-type), it is possible to design donor-acceptor (D-A) junctions in heterobilayer systems.

The second layer possesses a long-range order that is testified by the quite sharp molecular momentum maps reported in **Figure 4** with well-defined molecular azimuthal angles in the topmost and interface layers. The flat-lying adsorption geometry of the first layer is essentially preserved also in the second layer, where a tilt angle of 3 ± 5° is derived (see Figures S2 and S3, Supporting Information). Moreover, the adsorption geometry and azimuthal orientation are preserved from the first layer as no steric repulsion between the peripheral groups needs to be minimized due to their different nature in the heterojunctions. Analogously to homobilayers, the first layer decouples the second one from the substrate, resulting in the occupation of the sole HOMO (labeled as $HOMO_{bil}$ in Figure 4) and leaving the LUMO of the second layer unoccupied.
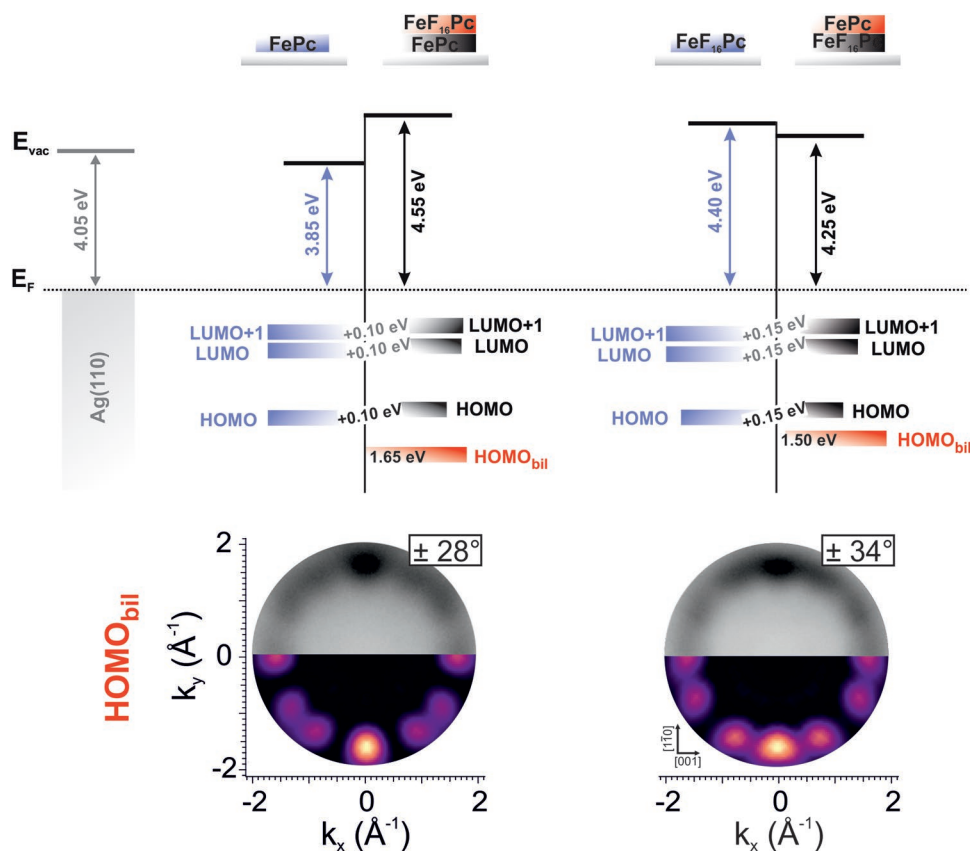
Figure 4. Energy level diagram referred to the clean Ag(110) substrate (top) and comparison between experimental and simulated momentum maps on the HOMO$_{bil}$ level (bottom) for heterobilayers deposited on Ag(110).

Interestingly, by assembling the n-type perfluorinated layer on top of the p-type FePc one, the work function of the system significantly increases (0.70 eV) and the levels of the layer in direct contact with the electrode are upshifted by 100 meV; the FeF$_{16}$Pc layer lowers the hole injection barrier, acting as the acceptor layer. The properties of this first heterojunction correspond to a donor–acceptor interface (n-p junction). The opposite is true when the order of the molecular layers is reversed. The deposition of a FePc layer on top of the perfluorinated first layer leads to the lowering of the work function by 0.15 eV, which corresponds to a donor character of the layer (p-n junction). The adsorption of the second layer still induces the upshift in the energy of the levels of the first layer.

3. Conclusion

In summary, we present how peripheral fluorination on FePc molecules (FeF$_8$Pc and FeF$_{16}$Pc) impacts the structure and electronic properties of the commensurate monolayers they form atop Ag(110). Remarkably, we underline, that the strong molecular surface interaction in the interface layer, independently of the degree of fluorination, can be exploited as a robust template for large-scale fabrication of well-defined layered p-n and n-p heterojunctions, depending on the stacking order. Significant are also the changes in the hole injection barrier that is

lowered as the degree of fluorination increases. Moreover, the steric repulsions define the adsorption geometry of the topmost layer in the fabricated homojunctions, where significant deviations of the azimuthal angles are observed for the fluorinated molecules, as revealed by PT. In the highly oriented molecular p–n heterojunction here designed, the hole injection barrier is effectively reduced, paving the way for its implementation in solar cells and/or light emitting diode (LED-type) devices.

4. Experimental Section

Synthesis: The blue powder of Iron(II) phthalocyanine (FeH$_{16}$Pc) was obtained from Alfa Aesar (purity 96%) and was sublimed to achieve further purification. Hexadecafluorinated iron(II) phthalocyanato (FeF$_{16}$Pc) was synthesized as described in the literature.[33] The newly synthesized octafluorinated iron(II) phthalocyanine (FeH$_8$F$_8$Pc) was prepared by slight modifications of the procedure reported for FeF$_{16}$Pc. Under an argon atmosphere, a solution (3 mmol, 0.4 mL) of iron(0) pentacarbonyl (Sigma–Aldrich, 99.9%) in 8 mL of 1-chloronaphthalene was dropwise added to a refluxing solution of 4,5-difluorophthalonitrile (synthesized as previously reported[34]) (12 mmol, 2 g) in 25 mL of 1-chloronaphthalene. The reaction mixture turned blue–green within an hour and was left under reflux overnight. Upon cooling, the reaction mixture was diluted with 50 mL

of hexane and filtered. The resulting solid was washed with hexane, acetone, and diethyl ether to obtain dark blue powder (yield 1.4 g, 66%), which was sublimed (10^{-3} mbar, 520 °C) for further purification. Elemental analysis: calculated for $C_{32}H_8F_8N_8Fe$: C 53.96, N 15.73, H 1.13, F 21.34, and Fe 7.84%. Found: C 54.2, N 15.7, H 1.32, F 21.02, and Fe 7.71%. MALDI-MS: m/z calculated for $C_{32}H_8F_8N_8Fe$ [M + 1e]$^-$ 712.009, found 711.999 (100% relative abundance). FT-IR (KBr, v / cm^{-1}): 2923 (w), 2851 (w), 1622 (m), 1475 (s), 1429 (m), 1340 (w), 1286 (w), 1181 (w), 1087 (m), 1041 (m), 882 (m), 822 (m), 748 (m), and 510 (w).

Sample Preparation: The clean Ag(110) surface was prepared by a standard procedure, cycles of Ar$^+$ ion sputtering at 2.0 keV followed by annealing at 800 K, while the surface quality was monitored by LEED. The molecules were thermally sublimated at 680 K (FePc), 690 K (FeF$_8$Pc), and 700 K (FeF$_{16}$Pc) from a homemade Knudsen cell type evaporator onto the silver substrate kept at room temperature. The chemical stoichiometry of the deposited molecules has been checked by measuring the F 1s, C 1s, and N 1s XPS spectra.

Matrix-assisted laser desorption ionization mass spectrum (MALDI-MS) was recorded on a Thermo Scientific MALDI LTQ Orbitrap XL mass spectrometer. The Fourier-transform infrared spectrum (FT-IR) was collected on a Bruker Vertex 70 spectrometer using KBr pellets of the compound. Elemental analyses (ICP-OES, IC, and CHN) were performed by the Central Institute for Engineering, Electronics, and Analytics (ZEA-3), Forschungszentrum Jülich GmbH (Jülich, Germany).

The valence band photoemission spectra, core levels and work function scans were acquired in normal emission geometry at the NanoESCA beamline of Elettra, using an electrostatic photoemission electron microscope (PEEM) setup.[35] The data were collected with a photon energy of 30 eV for the valence band, 380 eV (C 1s) and 515 eV (N 1s) for the core levels, with a total energy resolution of 50, 120, and 150 meV, respectively, using p-linearly polarized light impinging with an angle of 65° with respect to the surface normal. During the photoemission experiments, the sample was kept at 90 K.

Supporting Information

Supporting Information is available from the Wiley Online Library or from the author.

Conflict of Interest

The authors declare no conflict of interest.

Data Availability Statement

The data that support the findings of this study are available from the corresponding author upon reasonable request.

[1] T. Van Woudenbergh, P. W. M. Blom, J. N. Huiberts, *Appl. Phys. Lett.* **2003**, *82*, 985.

[2] I. H. Campbell, J. D. Kress, R. L. Martin, D. L. Smith, N. N. Barashkov, J. P. Ferraris, *Appl. Phys. Lett.* **1997**, *71*, 3528.

[3] B. De Boer, A. Hadipour, M. M. Mandoc, P. W. M. Blom, *Mater. Res. Soc. Symp. Proc.* **2005**, *871*, 189.

[4] G. Ashkenasy, D. Cahen, R. Cohen, A. Shanzer, A. Vilan, *Acc. Chem. Res.* **2002**, *35*, 121.

[5] S. C. Veenstra, A. Heeres, G. Hadziioannou, G. A. Sawatzky, H. T. Jonkman, *Appl. Phys. A: Mater. Sci. Process.* **2002**, *75*, 661.

[6] J. Lü, E. Delamarche, L. Eng, R. Bennewitz, E. Meyer, H. J. Güntherodt, *Langmuir* **1999**, *15*, 8184.

[7] S. D. Evans, E. Urankar, A. Ulman, N. Ferris, *J. Am. Chem. Soc.* **1991**, *113*, 4121.

[8] H. Ishii, K. Sugiyama, E. Ito, K. Seki, *Adv. Mater.* **1999**, *11*, 605.

[9] S. Kobayashi, T. Nishikawa, T. Takenobu, S. Mori, T. Shimoda, T. Mitani, H. Shimotani, N. Yoshimoto, S. Ogawa, Y. Iwasa, *Nat. Mater.* **2004**, *3*, 317.

[10] C. Reese, Z. Bao, *Mater. Today* **2007**, *10*, 20.

[11] X. Jiang, J. Dai, H. Wang, Y. Geng, D. H. Yan, *Chem. Phys. Lett.* **2007**, *446*, 329.

[12] T. L. Anderson, G. C. Komplin, W. J. Pietro, *J. Phys. Chem.* **1993**, *97*, 6577.

[13] W. J. Pietro, *Adv. Mater.* **1994**, *6*, 239.

[14] Y. Zhang, H. Dong, Q. Tang, S. Ferdous, F. Liu, S. C. B. Mannsfeld, W. Hu, A. L. Briseno, *J. Am. Chem. Soc.* **2010**, *132*, 11580.

[15] Q. Wang, J. Yang, A. Franco-Cañellas, C. Bürker, J. Niederhausen, P. Dombrowski, F. Widdascheck, T. Breuer, G. Witte, A. Gerlach, S. Duhm, F. Schreiber, *Nanoscale Adv.* **2021**, *3*, 2598.

[16] Y. Bai, F. Buchner, M. T. Wendahl, I. Kellner, A. Bayer, H. P. Steinrück, H. Marbach, J. M. Gottfried, *J. Phys. Chem. C* **2008**, *112*, 6087.

[17] B. Brena, C. Puglia, M. De Simone, M. Coreno, K. Tarafder, V. Feyer, R. Banerjee, E. Göthelid, B. Sanyal, P. M. Oppeneer, O. Eriksson, *J. Chem. Phys.* **2011**, *134*, 074312.

[18] T. Kroll, R. Kraus, R. Schönfelder, V. Y. Aristov, O. V. Molodtsova, P. Hoffmann, M. Knupfer, *J. Chem. Phys.* **2012**, *137*, 054306.

[19] P. F. Siles, T. Hahn, G. Salvan, M. Knupfer, F. Zhu, D. R. T. Zahn, O. G. Schmidt, *Nanoscale* **2016**, *8*, 8607.

[20] M. Casarin, M. Di Marino, D. Forrer, M. Sambi, F. Sedona, E. Tondello, A. Vittadini, V. Barone, M. Pavone, *J. Phys. Chem. C* **2010**, *114*, 2144.

[21] G. Zamborlini, D. Lüftner, Z. Feng, B. Kollmann, P. Puschnig, C. Dri, M. Panighel, G. Di Santo, A. Goldoni, G. Comelli, M. Jugovac, V. Feyer, C. M. Schneidery, *Nat. Commun.* **2017**, *8*, 1949.

[22] P. C. Rusu, G. Giovannetti, C. Weijtens, R. Coehoorn, G. Brocks, *J. Phys. Chem. C* **2009**, *113*, 9974.

[23] P. C. Rusu, G. Brocks, *J. Phys. Chem. B* **2006**, *110*, 22628.

[24] V. Feyer, M. Graus, P. Nigge, M. Wießner, R. G. Acres, C. Wiemann, C. M. Schneider, A. Schöll, F. Reinert, *Surf. Sci.* **2014**, *621*, 64.

[25] P. Puschnig, S. Berkebile, A. J. Fleming, G. Koller, K. Emtsev, T. Seyller, J. D. Riley, C. Ambrosch-Draxl, F. P. Netzer, M. G. Ramsey, *Science* **2009**, *326*, 702.

**ADVANCED
SCIENCE NEWS**

www.advancedsciencenews.com

**ADVANCED
FUNCTIONAL
MATERIALS**

www.afm-journal.de

[26] D. Brandstetter, X. Yang, D. Lüftner, F. S. Tautz, P. Puschnig, *Comput. Phys. Commun.* **2021**, *263*, 107905.

[27] K. Schönauer, S. Weiss, V. Feyer, D. Lüftner, B. Stadtmüller, D. Schwarz, T. Sueyoshi, C. Kumpf, P. Puschnig, M. G. Ramsey, F. S. Tautz, S. Soubatch, *Phys. Rev. B* **2016**, *94*, 205144.

[28] M. Graus, C. Metzger, M. Grimm, V. Feyer, P. Puschnig, A. Schöll, F. Reinert, *J. Phys. Soc. Jpn.* **2018**, *87*, 061009.

[29] I. Cojocariu, S. Carlotto, H. M. Sturmeit, G. Zamborlini, M. Cinchetti, A. Cossaro, A. Verdini, L. Floreano, M. Jugovac, P. Puschnig, C. Piamonteze, M. Casarin, V. Feyer, C. M. Schneider, *Chem. - Eur. J.* **2021**, *27*, 3526.

[30] P. Puschnig, *Organic Molecule Database*, http://143.50.77.12:5000, (accessed: July 2022).

[31] M. Tredwell, V. Gouverneur, *Compr. Chirality* **2012**, *1*, 70.

[32] M. Grimm, C. Metzger, M. Graus, M. Jugovac, G. Zamborlini, V. Feyer, A. Schöll, F. Reinert, *Phys. Rev. B* **2018**, *98*, 195412.

[33] J. G. Jones, M. V. Twigg, *Inorg. Chem.* **1969**, *8*, 2018.

[34] Z. Iqbal, A. Lyubimtsev, M. Hanack, *Synlett* **2008**, *15*, 2287.

[35] C. M. Schneider, C. Wiemann, M. Patt, V. Feyer, L. Plucinski, I. P. Krug, M. Escher, N. Weber, M. Merkel, O. Renault, N. Barrett, *J. Electron Spectrosc. Relat. Phenom.* **2012**, *185*, 330.

2208507 (8 of 8)